HAL
open science

# Comparative analysis of model reduction methods applied to building simulation benchmarks

Jordan Gauvrit, Guillaume Ansanay-Alex

## To cite this version:

Jordan Gauvrit, Guillaume Ansanay-Alex. Comparative analysis of model reduction methods applied to building simulation benchmarks. SSB2014, 9th International Conference on System Simulation in Buildings, Dec 2014, Liège, Belgium. 20 p. hal-01102181

**HAL Id: hal-01102181**

**https://cstb.hal.science/hal-01102181**

Submitted on 12 Jan 2015

**HAL** is a multi-disciplinary open access archive for the deposit and dissemination of scientific research documents, whether they are published or not. The documents may come from teaching and research institutions in France or abroad, or from public or private research centers.

L'archive ouverte pluridisciplinaire **HAL**, est destinée au dépôt et à la diffusion de documents scientifiques de niveau recherche, publiés ou non, émanant des établissements d'enseignement et de recherche français ou étrangers, des laboratoires publics ou privés.

# Comparative analysis of model reduction methods applied to building simulation benchmarks

Jordan Gauvrit[1], Guillaume Ansanay-Alex[1]*

(1) Centre Scientifique et Technique du Bâtiment, 84 avenue Jean Jaurès, Champs sur Marne, 77447 Marne la Vallée Cedex 2

## 1. ABSTRACT

Many research and development studies use virtual buildings represented by building thermal models at a detailed level. Such models need relatively long computation times for one-year simulations: the use of these tools is then often too time-consuming when it comes to compare technical solutions during the design stage. Model reduction methods allow models with shorter computation times to be synthesized. In this paper, the linear state-space representation of a whole model is extracted and a balanced truncation method is applied to it. The detailed models are built from the SIMBAD library, a Simulink library of building modeling components developed at CSTB. Both linear state-space and reduced order models ensure shorter computation times than the full detailed model. However, the choice of the order of the reduced model has an impact on the final results. The main strengths and weaknesses of using the linear state-space and reduced models built from the same detailed model are investigated. To this end, the physical descriptions of idealized test buildings provided by ASHRAE standard 140 for building simulation tools assessment are used, and the results obtained through the different approaches for computation time reduction are compared.

**Keywords:** thermal model, model order reduction, computation time, spectral analysis

## 2. INTRODUCTION

In 2012, commercial and residential buildings accounted for 44% of the final energy consumption in France and were responsible for 21% of Greenhouse Gas Emissions (Ademe, 2013). Among this consumption, heating and cooling systems stand for a large share (59%, (Ademe, 2013)). Therefore, reducing energy consumption requires the improvement of HVAC (Heating, Ventilation, Air Conditioning) systems efficiency. There are two ways to reach this goal. First, replacing old systems with high efficiency systems increases energy performance (Visier, 2008). Secondly, control methods allow to adapt the system operation to match occupants' needs or renewable energy production ((Visier, 2008),("Energy future, Think Efficiency," 2010)) and reduce energy waste.

Modelling innovative systems, complex distribution networks or control strategies for design and optimization purposes require detailed models and often short time steps. This can lead to long computations, hardly affordable during the design stage or for embedded control models.

The SIMBAD (SIMulator of Building And Devices) library, developed at CSTB (Husaunndee, Lahrech, Vaezi-Nejad, & Visier, 1997), is composed of a set of Matlab/Simulink components enabling user to build dynamic models of buildings, their systems and especially their control strategies. The components of this library will be used in this paper.

Simulating buildings with this level of detail leads to much longer computation times than static hourly models. In SIMBAD's case, an annual simulation of a mono-zone building takes

approximately 130s with a fixed time step $\Delta t = 20$s. Consequently, and considering even longer simulations when all production, distribution and emission systems are modelled, using such detailed models during the design stage may be difficult. It could then be useful to implement methods which reduce computation time while keeping sufficiently accurate results. The building envelope model considered in this paper will not take into account air transfer or non-linearized radiative transfers, but still shows a nonlinear behaviour regarding long wave radiations through windows.

The concern in this paper is to evaluate the performances of reduced models. On the one hand, the computation time saved with a reduced order model, and on the other hand, the accuracy difference between the results of detailed, linearized and reduced order models. Section 5 is dedicated to the problem of evaluating how well linearized or reduced order models perform with respect to the original detailed model.

In order to evaluate the detailed and reduced order building models on reference cases, the reference buildings used are those described by ASHRAE Standard 140-2001 ("ANSI/ASHRAE Standard 140-2001, Standard method of test for the evaluation of building energy analysis computer programs," 2001). It defines test procedures for evaluating capabilities of building energy programs. In fact, it gives a physical description of different buildings and the predictions from well-known programs (such as TRNSYS, DOE-2 or S3PAS) applied to them. Some of these test cases were implemented to compare synthesized models with the SIMBAD detailed model.

Section 3 will introduce the SIMBAD models used as the detailed modelling level. In section 4, the linearization and common model order reduction methods will be presented. Section 5 clarifies the mobilized benchmarks indicators. Benchmark results will be presented and discussed in section 6. Finally, a variant of the order reduction method will be tested to improve its performance in section 7.

## 3. DETAILED SIMBAD MODEL

The SIMBAD multi-zone building model is a white box model where each component (zones, walls, windows …) is described by a set of physical parameters. It includes a dynamic model of each wall surface and zone air temperature.

SIMBAD models are built using Simulink. Each component has inputs and outputs that are connected to create the whole model. Two cases are set up. The first one is the free floating case (indoor building temperature is not controlled, Figure 1). The second one is the regulated case (indoor building temperature is regulated using a PID controller, Figure 2).

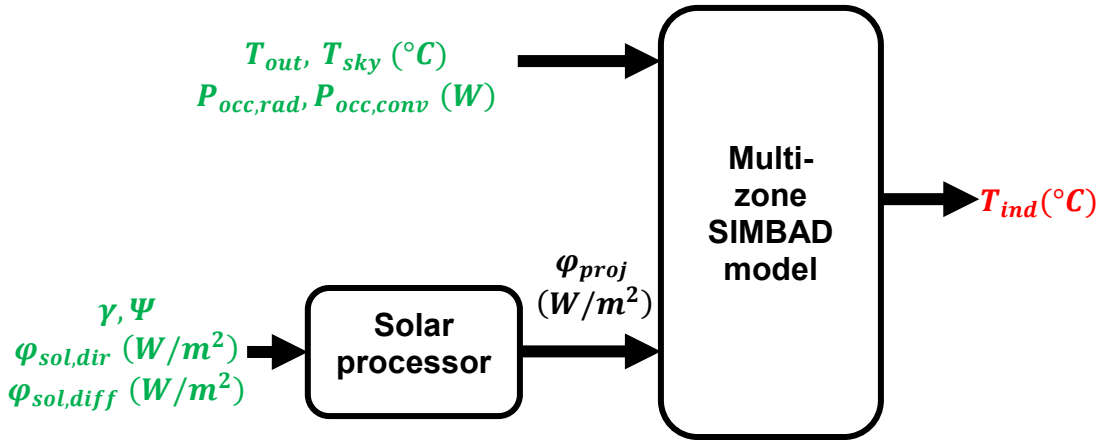




*Figure 1: Detailed SIMBAD model - Free floating case*

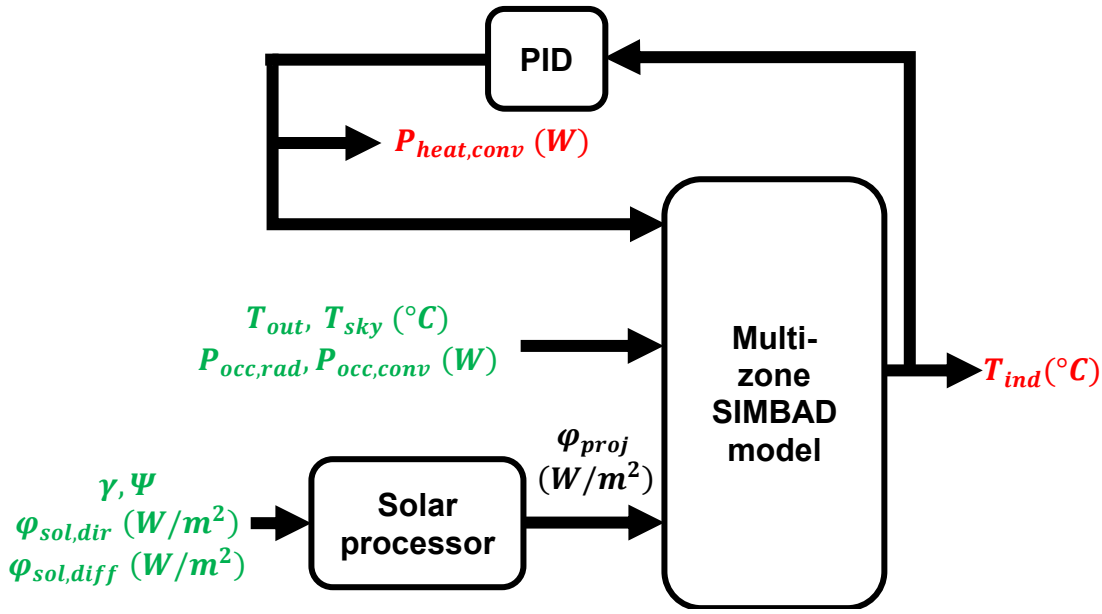


*Figure 2: Detailed SIMBAD model - Regulated case*

With:

$T_{out}$ : Outdoor temperature (°C)

$T_{sky}$ : Sky temperature (°C)

$P_{occ,rad}, P_{occ,conv}$ : Occupation convective power and occupation radiative power (W).

$\gamma, \Psi$ : Solar height and azimuth (°)

$\varphi_{sol,dir}, \varphi_{sol,diff}$ : Direct solar radiation and diffuse solar radiation ($W/m^2$)

$\varphi_{proj}$ : Solar radiation projected on building surfaces ($W/m^2$)

$T_{ind}$ : Indoor temperature (°C)

$P_{heat,conv}$ : Heating convective power (W). Positive for heating, negative for cooling.

The solar processor block projects solar flows on surfaces of the building envelope. This block uses many trigonometric functions and is as such strongly nonlinear.
The multi-zone block calculates indoor temperature by evaluating surface temperatures taking radiative, convective and conductive heat exchanges into account.
The PID controller computes the heating convective power in order to reach the setpoint value. It is strongly nonlinear and won't be subject to model order reduction.
In the rest of this paper, the detailed model will be represented by the letter D.

## 4. COMPUTATION TIME AND MODEL ORDER REDUCTION TECHNIQUES

### 4.1 Linearization

Linearization replaces any block or set of blocks with a State Space Model (SSM) block. Matlab function *linmod* extracts the SSM from a component by a numerical perturbation and gives four matrices: $A, B, C, D$. They allow writing the state space representation (1) of the model called in the following the linearized model (L).

$$\begin{aligned} \dot{T}(t) &= AT(t) + BU(t) \\ Y'(t) &= CT(t) + DU(t) \end{aligned} \tag{1}$$

With:

| | |
|---|---|
| $T(t)$: State vector | $A$: State matrix |
| $Y'(t)$: Output vector | $B$: Input matrix |
| $U(t)$: Input vector | $C$: Output matrix |
| | $D$: Feedforward matrix. In this case, it is always null. |

This technique works by nature without any loss of precision when blocks are linear.

There are two ways to apply this technique to the detailed building model:

- The first one is the linearization of the multi-zone building block only. This block is then replaced with a SSM block but the solar processor is maintained. The resulting SSM block has 23 inputs.
- The second one is the linearization of the assembly between the solar processor and the multi-zone block. As the solar processor is not linear, a simplification is made to make it linear: the sun position is set to a constant and becomes a model parameter. Then, the assembly is replaced with a SSM block. Solar radiations are adjusted to fit the initial solar radiation projected on the window. This SSM block requires 8 inputs.

## 4.2 Model order reduction

After projecting (1) on a particular basis, the system is truncated (2).

$$\begin{aligned} \dot{\tilde{T}}(t) &= \tilde{A}\tilde{T}(t) + \tilde{B}U(t) \\ \tilde{Y'} &= \tilde{C}\tilde{T}(t) \end{aligned} \tag{2}$$

In the following parts, the notation $Y'$ will stand for the outputs of linearized models as well as the outputs of the reduced order model.

The order of (2) has decreased from (1). Several methods performing this reduction are available . One of the first method was the balanced truncation and appeared in the early 80's. It was described by B.C. Moore in (Moore, 1981). Other methods followed in the same decade as the Hankel-norm reduction of Glover (Curtain & Glover, 1985) or whether the proper orthogonal decomposition described by Sirovich (Sirovich, 1987). Finally, in the 90's, two other methods came out. The first one was explained by P. Feldmann in (Feldmann & Freund, 1995) and was related to Krylov subspaces and Padé approximation. The second one is called PRIMA and was the subject to the paper (Odabasioglu, Celik, & Pileggi, 1997). In this study, the balanced truncation is used. It has been applied in thermal building modelling since the mid-1990s. Dautin's works (Dautin, 1997) or Déqué's works (Déqué, Delille, & Dautin, 1997) can be quoted. More recently, other studies like (Kim & Braun, 2012) used this technique.

The main idea is to delete states that have a small sensitivity to inputs (controllability) and a small impact on outputs (observability). The controllability gramian $W_c$ (resp. observability gramian $W_o$) characterizes the state's controllability (resp. observability). It is shown (Bruq & Folliot, 1988) that they can be calculated by Lyapunov equations (3):

$$\begin{aligned} AW_c + W_cA^T + BB^T &= 0 \\ A^TW_o + W_oA + C^TC &= 0 \end{aligned} \tag{3}$$

$W_c$ and $W_o$ depend on the basis where (1) is represented. It should be noted that a state can be sensitive to inputs and have a small impact on outputs at the same time. States thus cannot be deleted by considering the gramians only. Using a balanced representation overcomes this obstacle.

It consists in applying a transform $T(t) = PX(t)$ to (1) such that the gramians of system (4) are equal.

$$\begin{aligned} \dot{X}(t) &= P^{-1}APX(t) + P^{-1}BU(t) \\ Y'(t) &= CPX(t) \end{aligned} \tag{4}$$

Palomo (Palomo, 2011) gives steps to establish $P$ :

- 1st step: Computation of $W_c$ and $W_o$ with (3)
- 2nd step: Calculation of $R$ with Cholesky decomposition :

$$W_c = R\,R^T \tag{5}$$

where $R$ is a lower triangular matrix.

- 3rd step: Diagonalization of $R^T W_o R$ (symmetric, positive definite) obtained by solving the following symmetric eigenvalues/eigenvectors problem:

$$R^T W_o R = U\Sigma^2 U^T \tag{6}$$

where Σ is a diagonal matrix and $U$ is such that $U\,U^T = I$.

- 4th step: Calculation of $P$ :

$$P = R\,U\,\Sigma^{-1/2} \tag{7}$$

Then, (4) can be reduced by deleting the less influential states, leading to (2). The reduction order is the number of remaining states.

This model will be called (R) for Reduced order model. A reduced order model of order 5 will be denoted R5.

## 5. BENCHMARKING

### 5.1 Computation time notation

The reference time is obtained by the simulation time of D. As regards L and Rx models, the time spent to reduce the detailed model is taken into account.

### 5.2 An a priori evaluation

The "quality" of R can be evaluated by analyzing its state space representation without the aid of a simulation. Palomo ((Palomo, 2011), (Palomo, Bonnefous, & Déqué, 1997)) defines an index of the spectral quality called $\eta_i(\omega)$. For each output $i$, it gives the relative error (between L and R) according to input frequency $\omega$.

To achieve this target, transfer function matrix of the linearized (resp. reduced order) model $G(\omega)$ (resp. $\tilde{G}(\omega)$) is calculated by :

$$\begin{aligned} G(\omega) &= C(j\omega I - A)^{-1}Bj\omega \\ \tilde{G}(\omega) &= \tilde{C}\left(j\omega I - \tilde{A}\right)^{-1}\tilde{B}j\omega \end{aligned} \tag{8}$$

Then, $\eta_i(\omega)$ is determined by:

$$\eta_i(\omega) = \frac{\sum_{j=1}^{j=p} \left|G_{ij}(\omega) - \tilde{G}_{ij}(\omega)\right|^2}{\sum_{j=1}^{j=p} \left|G_{ij}(\omega)\right|^2} \tag{9}$$

With:

$p$ : Number of inputs

$G_{ij}(\omega)$ (resp. $\tilde{G}_{ij}(\omega)$) : Transfer function of the $i^{\text{th}}$ output from the $j^{\text{th}}$ input. It belongs to the matrix $G(\omega)$ (resp. $\tilde{G}(\omega)$).

Thus, the reduction order can be chosen by setting a risk tolerance threshold on the index.

## 5.3 An evaluation by simulation

Also, L and Rs have to be compared with the detailed model. A one year simulation is performed for each model and the results are studied. The gap between detailed model outputs and reduced model outputs, written $e(t)$, is called the reduction error.

*Statistical analysis*

A first statistical analysis of $e(t)$ by calculating the mean and the standard deviation will be made. Moreover, heating power and cooling power results will be integrated:

- over one hour time steps to compare maximum peaks (ASHRAE standard indicator)
- over a year to compare annual consumptions

*Spectral analysis*

Secondly, a spectral analysis of $e(t)$ will be performed. It is especially described for building thermal modeling in (Dautin, 1997) or (Ramdani et al., 1997). It aims at evaluating the dynamic behavior of reduced models in comparison with the detailed model.

The power spectral density (PSD) of $e(t)$, noted $S_{ee}(f)$ and calculated by (10), shows how the energy of the signal is distributed over the different frequencies. It must not be confused with the energy of the physical quantity.

$$S_{ee}(f) = |\hat{e}(f)|^2 \tag{10}$$

where $\hat{e}(f)$ is the Fourier transform of $e(t)$.

The links between reduction error and model inputs are also investigated. Spectral coherence of $e(t)$ and an input signal $x(t)$ gives information about these. It is noted $K_{ex}^2(f)$ and calculated by (11). It expresses the linear correlation between both signals according to the frequency.

$$K_{ex}^2(f) = \frac{|S_{ex}(f)|^2}{S_{ee}(f)S_{xx}(f)} \tag{11}$$

Where $S_{ex}(f)$ is the cross spectral density (CSD) of both signals and is determined by :

$$S_{ex}(f) = \hat{e}(f)\hat{x}(f)^* \tag{12}$$

Coherence allows comparing the influence of each input on reduction error of one reduced model. However, it is not a sufficient tool for comparing the influence of one input over two models. The partial coherence method (PCM) is an answer to this problem.

PCM offers a decomposition of $S_{ee}(f)$ such as:

$$S_{ee}(f) = \sum_{j=1}^{p} \Lambda_j\,(f) + Z(f) \tag{13}$$

With:

$\Lambda_j(f)$ : Linear contribution of the $j^{th}$ input to $S_{ee}(f)$

$Z(f)$ : Unexplained part of $S_{ee}(f)$

(Ramdani et al., 1997) provides equation (14). Knowing the contribution of the $j^{th}$ input requires to know the contribution of the $(j-1)^{th}$ input. The whole contribution computation is then an iterative process. The computation scheme, drawn on the Figure 3, is established in the case of a model with 3 inputs.

$$\Lambda_j(f) = K^2_{je/1..j-1}(f) S_{ee/1..j-1}(f) \tag{14}$$

With:

$K^2_{je/1..j-1}(f)$ : Coherence between the $j^{th}$ input and $e(t)$ after removing the linear contributions of the $1^{st}$ input to the $(j-1)^{th}$ input. It is called partial coherence.

$S_{ee/1..j-1}(f)$ : PSD of $e(t)$ after removing the linear contributions of the $1^{st}$ input to the $(j-1)^{th}$ input.

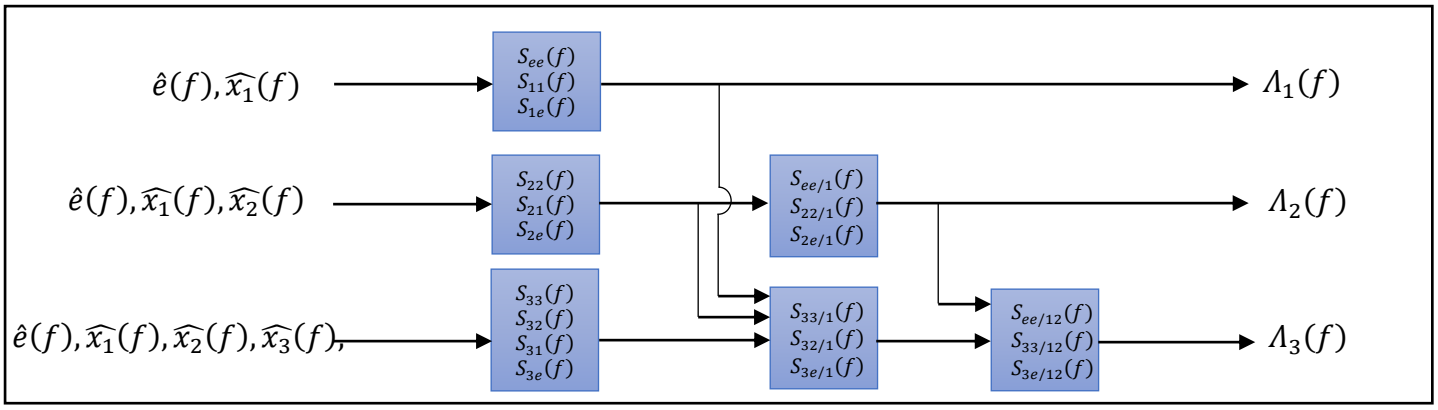


*Figure 3: Computation scheme of input's contribution to $S_{ee}(f)$ by PCM method in case of a 3 inputs model.*

In Figure 3, terms like $S_{XY/1..j}(f)$ and partial coherence $K^2_{je/1..j-1}(f)$ are calculated by:

$$S_{XY/1..j}(f) = \frac{S_{jj/1..j-1}(f) S_{XY/1..j-1}(f) - S_{Xj/1..j-1}(f) S_{jY/1..j-1}(f)}{S_{jj/1..j-1}(f)}$$
$$K^2_{je/1..j-1}(f) = \frac{\left|S_{je/1..j-1}(f)\right|^2}{S_{jj/1..j-1}(f) S_{ee/1..j-1}(f)} \tag{15}$$

This pattern is generally applicable with any number of inputs. In addition, it should be noticed that the order in which inputs are sorted affects the computed values of contributions. For instance, considering two inputs which are severely correlated with $e(t)$ ($K^2_{e1}(f) \sim 1$ and $K^2_{e2}(f) \sim 1$). If the contribution of input 1 is calculated at first, then $\Lambda_1(f) = K^2_{e1}(f) \sim 1$ and

$\Lambda_2(f)\sim 0$. Now, if the contribution of input 2 is calculated at first, then $\Lambda_2(f) = K_{e2}^2(f)\sim 1$ and $\Lambda_1(f)\sim 0$. However, the unexplained portion stays the same regardless of the order of inputs. For the following parts, the order of inputs will be fixed for the comparison of models. Finally, results of the spectral analysis will be summed up by frequency bands. They are defined by the observation of the PSD of a signal. Here, (Figure 4), the signal is the error on the indoor temperature prediction of L. Four frequency bands are chosen:

- VLF band: Very low frequency band (between 0 to $(48h)^{-1}$). It describes quasi-static behaviour
- LF band: low frequency band (between $(48h)^{-1}$ to $(16h)^{-1}$). It describes slow dynamic behaviour.
- HF band: high frequency band (between $(16h)^{-1}$ to $(9h)^{-1}$). It describes medium dynamic behaviour.
- VHF band: very high frequency band (superior to $(9h)^{-1}$). It describes fast dynamic behaviour.

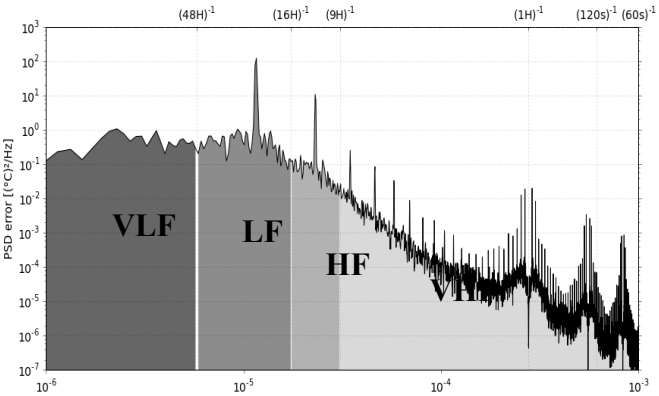


*Figure 4: PSD signal example and frequency bands*

The portion of the energy of the signal $e(t)$ contained in the frequency band $B_i$ is noted $s_{ee,B_i}$and is calculated by:

$$\boldsymbol{s_{ee,B_i}} = \frac{\int_{B_i} \boldsymbol{S_{ee}(f)df}}{\sum_{i=1}^{i=4} \int_{B_i} \boldsymbol{S_{ee}(f)df}} \tag{16}$$

The part of the energy of the signal $e(t)$ explained by input $j$, contained in the frequency band $B_i$, is noted $\lambda_{j,B_i}$ and is calculated by:

$$\lambda_{j,B_i} = \frac{\int_{B_i} \boldsymbol{\Lambda_j(f)df}}{\int_{B_i} \boldsymbol{S_{ee}(f)df}} \tag{17}$$

The portion which cannot be explained by the inputs is called the unexplained part. A graphic representation of these quantities is available in section 6.2.3.

# 6. RESULTS

## 6.1 Hypotheses

### *6.1.1 Test cases*

In this paper, ASHRAE test cases used are case600FF, case900FF, case600 and case900. They reflect a mono-zone building with two south-oriented windows (Figure 5). Simulations are conducted over a one year period with a fixed time step $\Delta t = 20$s.

The weather data come from the ASHRAE standard and match the weather in Denver, Colorado, USA.

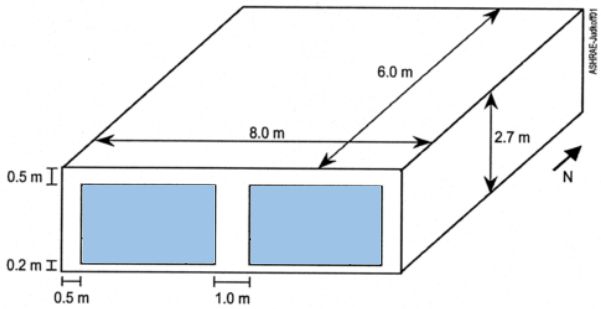


*Figure 5: Building geometry of cases*

*Table 1: Cases' names*

| | Low mass | High inertia |
|---|---|---|
| **Free floating** | case600FF | case900FF |
| **Regulation** | case600 | case900 |

According to the case, envelope inertia and indoor temperature control change (Table 1). In particular:

- Free floating case: indoor temperature is not controlled
- Regulation case: indoor temperature is regulated. The heating set-point is 20°C and the cooling set-point is 28°C.

### *6.1.2 Choice of reduced model orders*

The spectral index, defined in subsection 5.2, is a useful tool to anticipate the quality of the results of Rs according to reduction order. It should be reminded that the spectral index is calculated by comparing L and Rs. Figure 6 and Figure 7 show indices estimated for case600 and case900 with SSM block including 23inputs or 8inputs. On each chart, a gap of the index may be observed between order5 and order6. Then, R6 and L make very close predictions. In the following parts, the results of R2, R4 and R6 will be exposed.

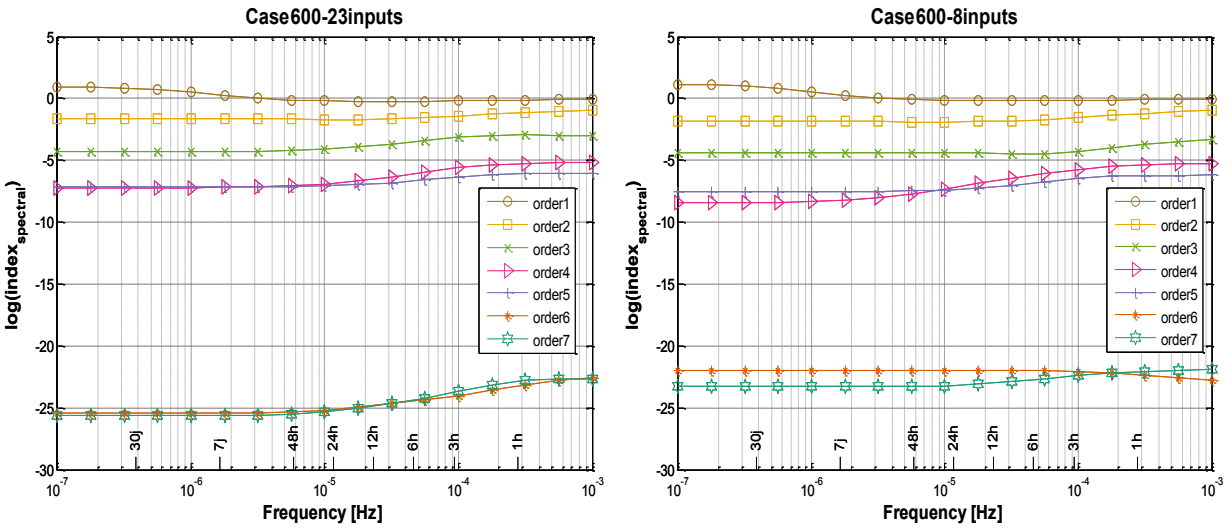


*Figure 6 : Spectral indices according to model input numbers - Case600*

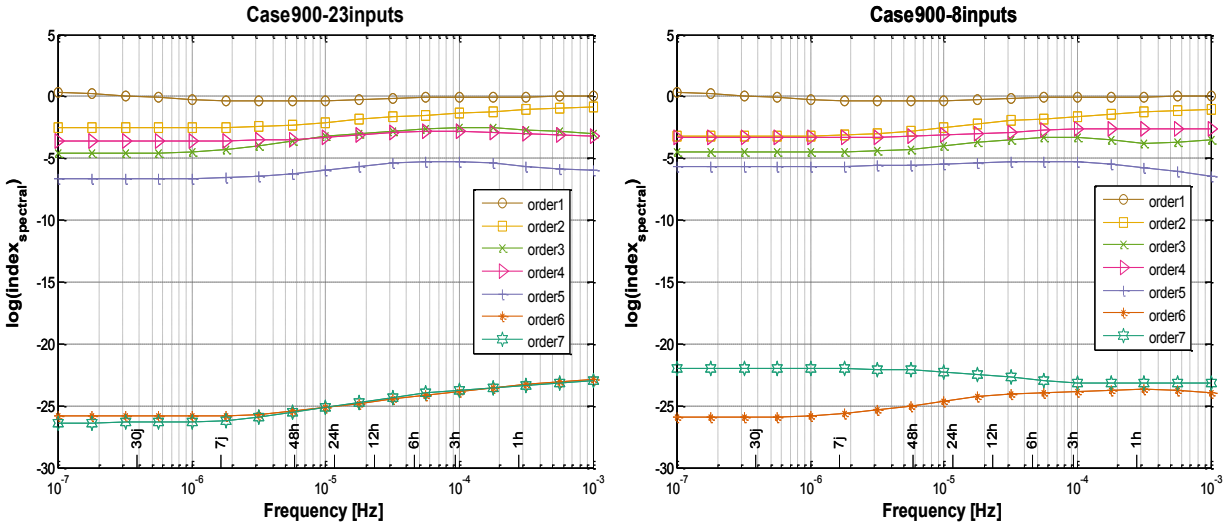


*Figure 7: Spectral indices according to model input numbers – Case900*

## 6.2 Free floating cases

### *6.2.1 Computation times*

Computation times are shown in Table 2. L with 23 inputs (resp. 8 inputs) roughly divides by two (resp. by three) the simulation time. In fact, for D, Matlab computes the outputs of each subcomponent at each time step: it considers the detailed model as a time variant system. In L's case, time invariance property is ensured through the linearization stage. That's why this computation is simplified and faster.

Secondly, it can be noticed that 8-input models have shorter computation times than 23-input models. Indeed, the solar processor block has been linearized and has been "included" in the SSM block. Moreover, a SSM with 8 inputs is smaller than a SSM with 23 inputs.

*Table 2: Computation times - Free floating cases*

| Case | D | L | R2 | R4 | R6 |
|---|---|---|---|---|---|
| Case600FF/8inputs | 110,45s | 29,71s | 28,29s | 28,61s | 30,45s |
| Case600FF/23inputs | | 55,97s | 53,90s | 55,63s | 60,33s |
| Case900FF/8inputs | 108,41s | 28,65s | 26,26s | 27,06s | 27,70s |
| Case900FF/23inputs | | 55,59s | 53,62s | 55,03s | 57,05s |

Finally, Rs have results very close to L. It seems to be a paradox because matrices of Rs are smaller than L's ones. In fact, matrices of L are sparse (Figure 8) and Matlab optimizes the solving of SSM according to the number of null coefficient inside matrices. Then, even if sizes of L matrices are bigger, their sparsity must be taken into account to understand computation times.

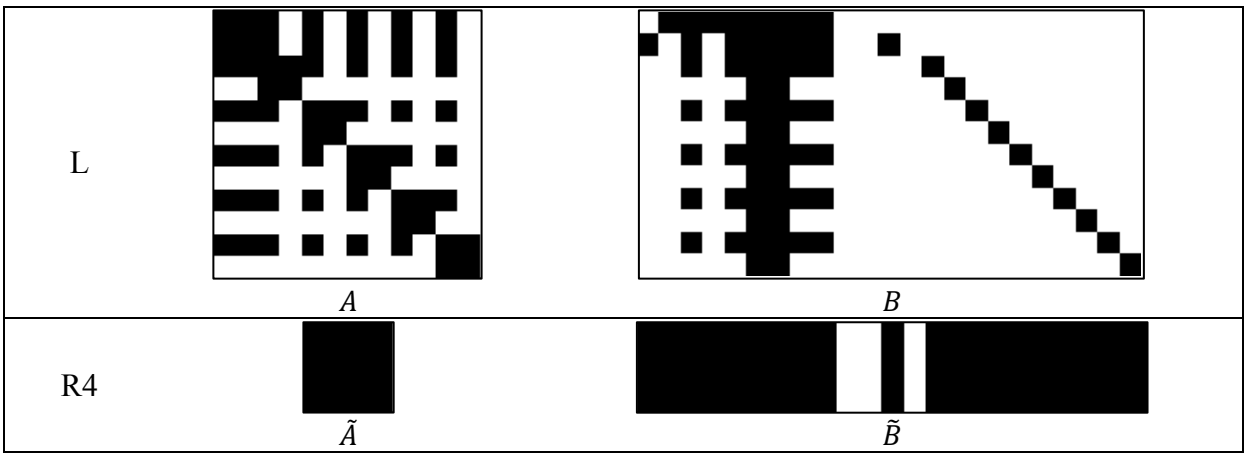


*Figure 8: Sparsity of matrices for L and R4*

### *6.2.2 Statistical analysis*

Differences between indoor temperature prediction of D with L and Rs have been calculated. Means and standard deviation of the reduction errors are shown in Table 3 and Table 4.

As could be expected, L and R6 give very similar results. The mean of the difference between their results is close to $10^{-11}$ °C.

*Table 3: Mean of reduction error (°C) - Free floating cases*

| Case | L | R2 | R4 | R6 |
|---|---|---|---|---|
| Case600FF/8inputs | -3.17e-02 | -2.77e+00 | -2.66e-02 | -3.17e-02 |
| Case600FF/23inputs | -8.00e-06 | -3.82e+00 | -2.27e-03 | -8.00e-06 |
| Case900FF/8inputs | -2.90e-02 | -9.91e-01 | -7.51e-01 | -2.90e-02 |
| Case900FF/23inputs | -5.12e-06 | 1.31e+00 | -4.24e-01 | -5.12e-06 |

Results of L with 8 and 23 inputs are close to D. However, R2s give results far from D. Models with 23 inputs give generally better results than model with 8 inputs. This probably stems from an exaggerated simplification of projected solar radiations made in the 8-input model.

*Table 4: Standard deviation of reduction error (°C) - Free floating cases*

| Case | L | R2 | R4 | R6 |
|---|---|---|---|---|
| Case600FF/8inputs | 5.09e-01 | 1.49e+00 | 5.09e-01 | 5.09-01 |
| Case600FF/23inputs | 7.27e-03 | 2.22e+00 | 7.24e-03 | 7.27-03 |
| Case900FF/8inputs | 3.60e-01 | 3.89e-01 | 3.34e-01 | 3.60-01 |
| Case900FF/23inputs | 6.03e-04 | 5.33e-01 | 1.45e-01 | 6.03-04 |

The same observations as before can be made about dispersion of reduction errors, in terms of difference between 8-input models and 23-input models, and the evolution of dispersion according to reduction order.

### *6.2.3 Spectral analysis*

For each model, the decomposition of the reduction error was calculated thanks to (16) (energy of the residual in a frequency band) and (17) (energy explained by each specific input in a frequency band). The inputs are meteorological variables (outdoor temperature, sky temperature, diffuse and direct solar radiations). Table 5 (resp. Table 6) shows results for

case600FF (resp. case 900FF). In these graphs “Inex” denotes the energy unexplained by inputs.

Less than 10% of the reduction error is not explained by the chosen inputs. Moreover, the reduction error is mainly connected with static and slow dynamic behaviors (more than 80% of the signal’s energy, i.e. the error). Then, climatic data are relevant to explain the error.

*Table 5: Decomposition of reduction error - Free floating, case600FF*

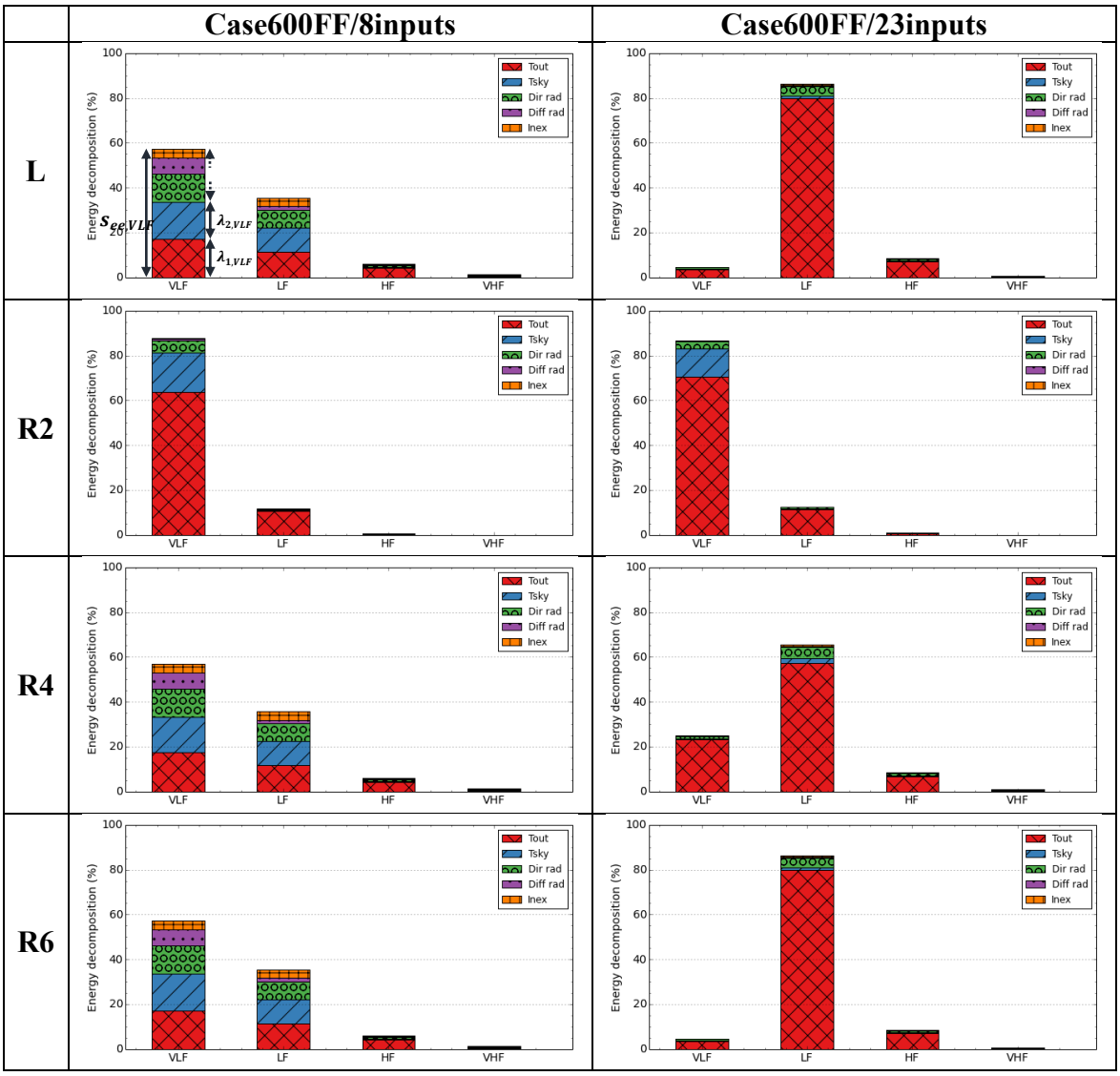


Concerning case600FF, the decomposition of reduction error of L with 8 inputs shows an important effect of meteorological inputs linked to radiative transfers (with regard to decomposition of the model with 23 inputs). The same observation can be made for R4 and R6. Here shows up the effect of the simplification of the solar processor for the 8 inputs model.

The decomposition of R2 looks similar for both models. The effect of radiative transfer modeling is then pretty close and they produce equivalent dynamic behaviors.

It can be noticed that the VLF part of the reduction error decreases with the reduction order being higher.

Concerning case900FF, reduction error is more connected with static behavior than in case600FF. That shows the effect of building inertia on the reduction error.

Also, an important effect of inputs linked to radiative transfer on models with 8 inputs can be observed, which points towards the simplification made to the solar processing part.

Table 6: Decomposition of reduction error - Free floating, case900FF

| | Case900FF/8inputs | Case900FF/23inputs |
|---|---|---|
| **L** | 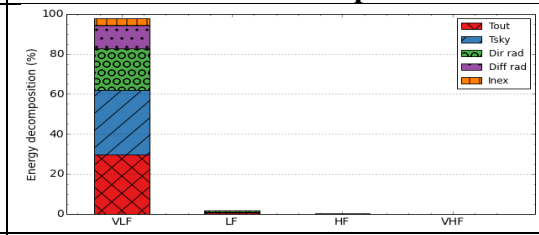 | 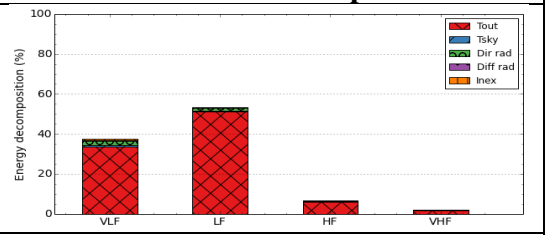 |
| **R2** | 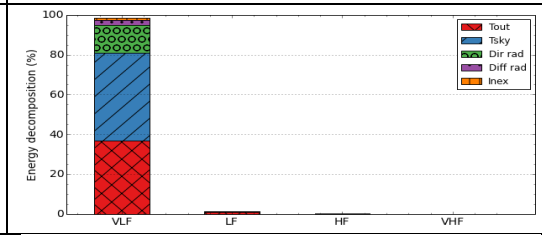 | 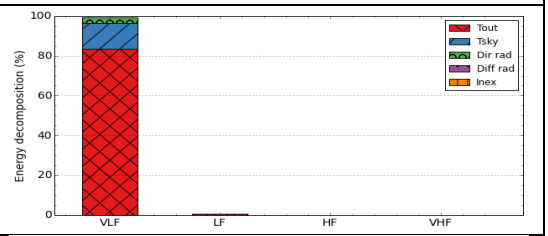 |
| **R4** | 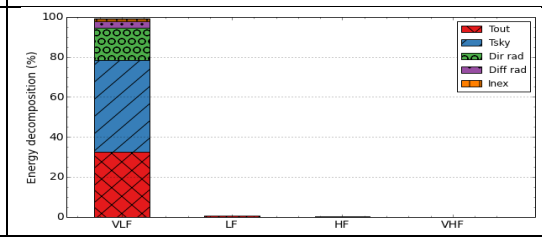 | 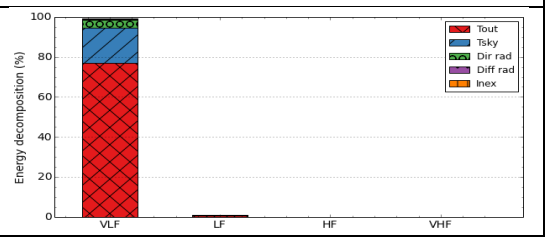 |
| **R6** | 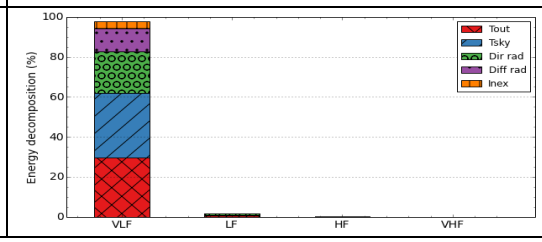 | 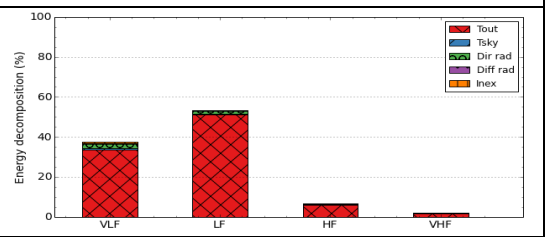 |



## 6.3 Regulation cases

### *6.3.1 Computation times*

Computation times of regulation cases are shown in Table 7. The same observations as the previous case can be made about time savings and reduction methods.

*Table 7: Computation times - Regulation cases*

| Case | D | L | R2 | R4 | R6 |
|---|---|---|---|---|---|
| Case600/8inputs | 138,67s | 55,85s | 52,83s | 53,88s | 57,22s |
| Case600/23inputs | | 83,78s | 84,67s | 85,37s | 87,53s |
| Case900/8inputs | 147,94s | 55,59s | 53,62s | 55,03s | 57,12s |
| Case900/23inputs | | 86,46s | 83,83s | 86,59s | 88,06s |

### *6.3.2 Statistical analysis*

Differences between output predictions of D and L and Rs have been calculated. Mean and standard deviation of the reduction error on indoor temperature are shown in Table 8 and Table 9.

Two behaviors can be distinguished in the regulation case. The first one is the period when indoor temperature is controlled (heating or cooling period). The temperature is quasi constant. The second one is a free floating period. When the indoor temperature is between 20°C and 28°C (the two set-points), indoor temperature is not controlled. In fact, periods when indoor temperature has a static behavior limit the value of reduction error. Then, the mean is often lower than free floating case. Mean reduction errors higher than in the free floating case are underlined in the following tables.

*Table 8: Mean of reduction error on indoor temperature (°C) – Regulation cases*

| Case | L | R2 | R4 | R6 |
|---|---|---|---|---|
| Case600/8inputs | 2.00e-02 | -3.06e-01 | 2.07e-02 | 2.00e-02 |
| Case600/23inputs | 2.75e-04 | -4.58e-01 | -2.04e-05 | 2.75e-04 |
| Case900/8inputs | -1.80e-02 | -2.62e-01 | -1.78e-01 | -1.80e-02 |
| Case900/23inputs | 4.89e-05 | 2.60e-01 | -7.04e-02 | 4.89e-05 |

About the standard deviation, the same observations can be made about models with 8 inputs. However, in this case, the reduction error of models with 23 inputs is more scattered than free floating case.

*Table 9: Standard deviation of reduction error on indoor temperature (°C) - Regulation cases*

| Case | L | R2 | R4 | R6 |
|---|---|---|---|---|
| Case600/8inputs | 1.51e-01 | 5.76e-01 | 1.56e-01 | 1.51e-01 |
| Case600/23inputs | 4.38e-02 | 8.14e-01 | 6.20e-02 | 4.38e-02 |
| Case900/8inputs | 1.42e-01 | 4.00e-01 | 2.45e-01 | 1.42e-01 |
| Case900/23inputs | 2.69e-02 | 3.39e-01 | 1.13e-01 | 2.69e-02 |

Finally, these statistical indicators show predictions of L and Rs are pretty close to those of D.

For confirming this trend, annual consumptions and hourly peaks of heating and cooling system have calculated. Results are presented in Table 10 and Table 11.

In the background of each chart, the banner represents the score interval of the set of tools presented in the ASHRAE standard. The dotted line is the mean result of the standard.

R2, with 23 or 8 inputs, gives results outside the banner. It can be noticed for the cooling and the heating consumptions in Case600. However, all other models make coherent predictions with the standard.

Finally, R4 seems to be a sufficient model to predict consumptions and hourly peaks close to those of D. In fact, a maximum deviation of 3.2% can be found between R4 and D results. It concerns cooling peak of a model with 8 inputs.

*Table 10 : Consumptions and hourly peaks - Case600*

| | Heating | Cooling |
|---|---|---|
| **Consumption** | 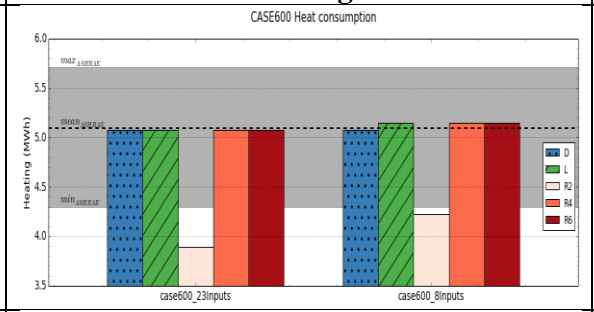  | 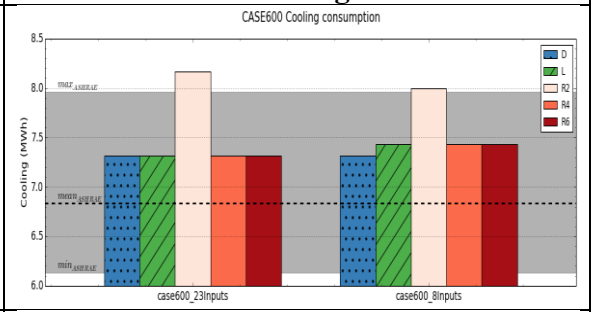  |
| **Hourly peak** | 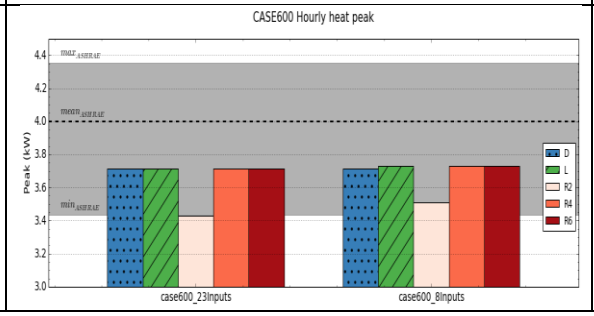  | 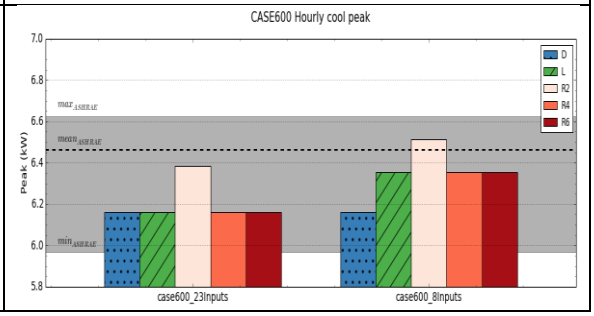  |

*Table 11 : Consumptions and hourly peaks results – Case900*

| | Heating | Cooling |
|---|---|---|
| **Consumption** | 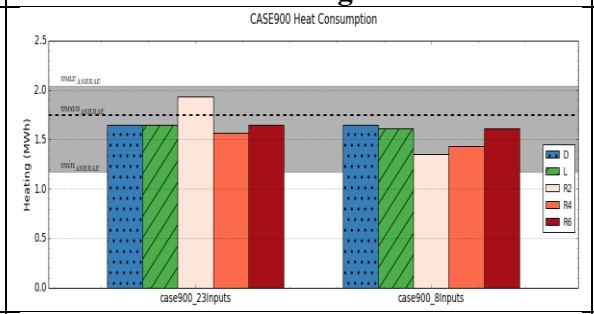  | 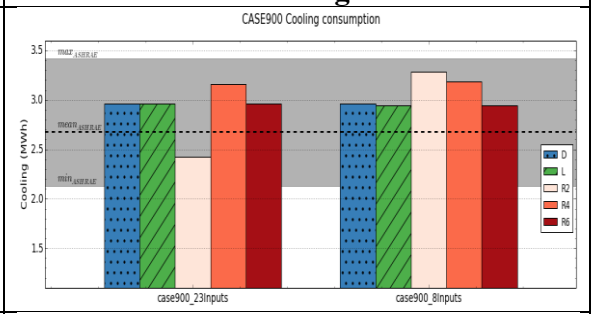  |
| **Hourly peak** | 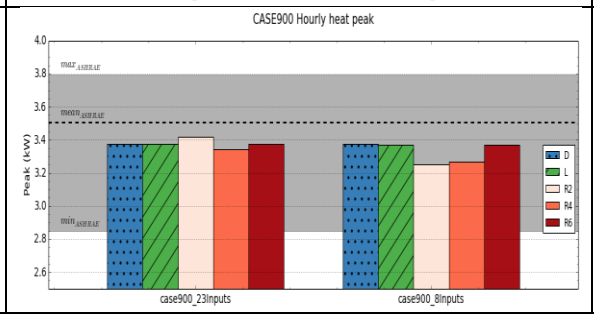  | 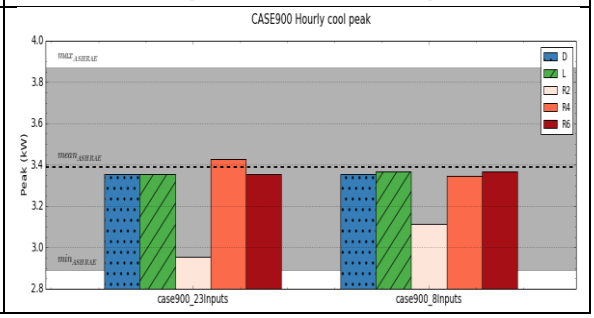  |

### *6.3.3 Spectral analysis*

The decomposition of indoor temperature reduction error has been calculated for each model. It is shown in Table 12 for case600 and in Table 13 for case900. The effect of heating convective power has been added to the analysis.

In case600, reduction error of L, R4 and R6 is mainly in the very high frequency band: this could be expected considering that the VHF band spans frequencies higher than (9h). Decompositions are close between the model with 8 inputs and the model with 23 inputs but the simplification on the solar processor in the 8-input model creates low frequency error. The

unexplained part is quite important (more than 10% here). It can be noticed all the inputs have the same contribution on the reduction error (around 16%).

In case900, a higher order model (R6) is necessary to get rid of the reduction errors showing up in the VLF, LF and HF frequency bands. The errors on solar heat gain implied by the simplification of the solar processor have much more impact than in the lighter case600.

In the following graphs, Pcl denotes the convective power input.

*Table 12 : Decomposition of indoor temperature reduction error - Regulation, case600*

| | **Case600/8inputs** | **Case600/23inputs** |
|---|---|---|
| **L** | 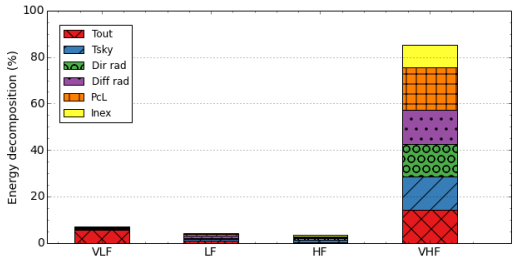  | 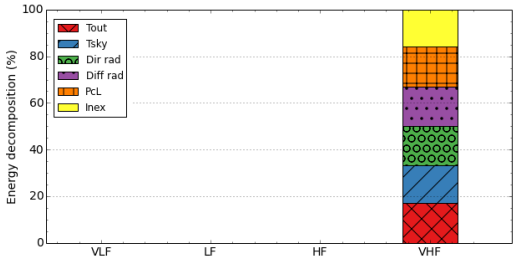  |
| **R2** | 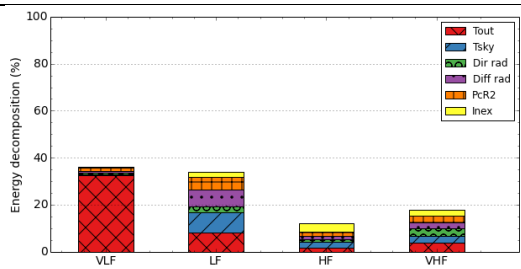  | 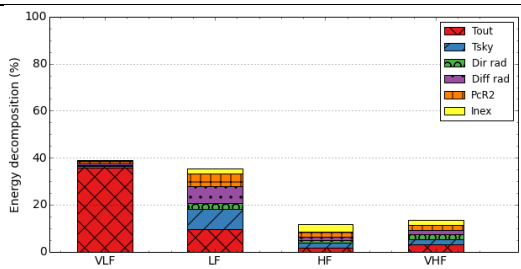  |
| **R4** | 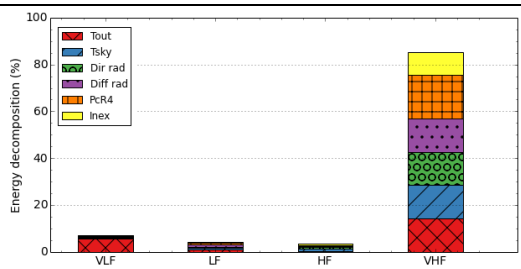  | 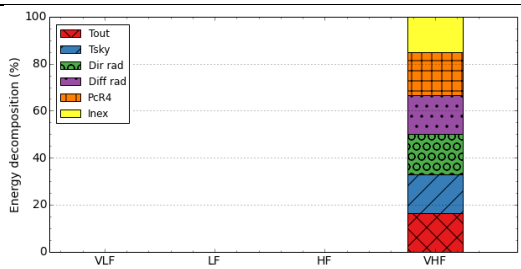  |
| **R6** | 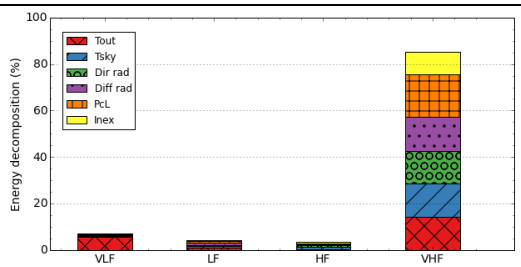  | 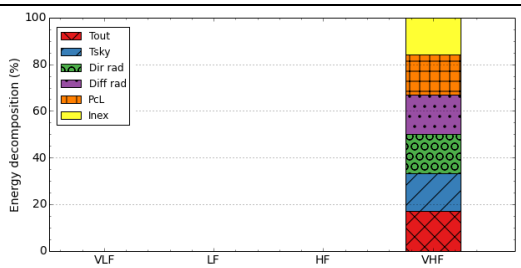  |

*Table 13: Decomposition of indoor temperature reduction error - Regulation, case900*

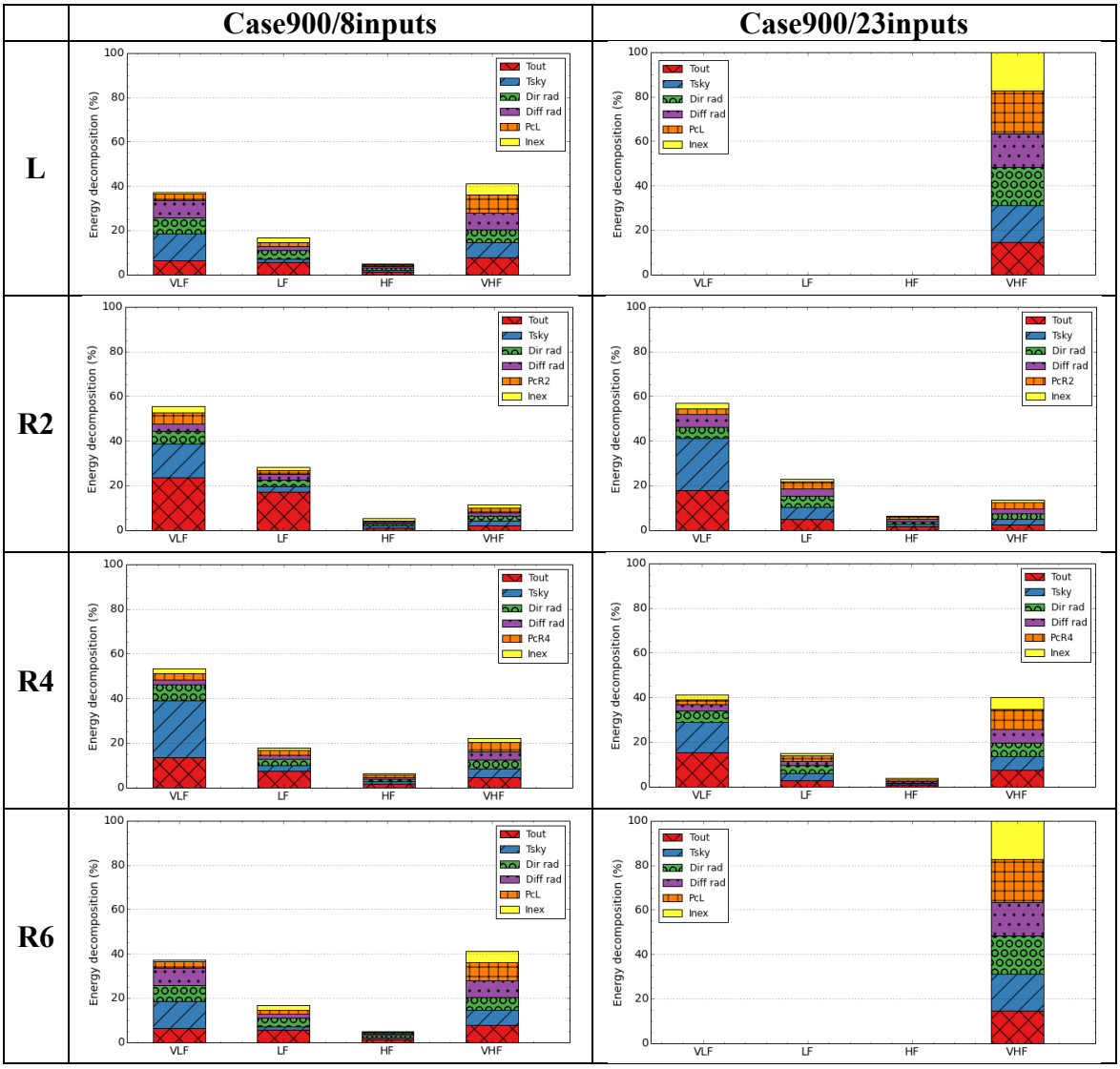


## 7. A VARIANT OF BALANCED TRUNCATION

### 7.1 Description

With a sufficient order, balanced truncation gave results close to L. However, computation time does not decrease because, contrary to L, matrices of reduced order models are not sparse and the number of inputs is large. Recent methods such as SVDMOR and RecMOR (Feldmann & Liu, 2004) or TermMerg (Liu, Tan, & McGaughy, 2007) are able to reduce model with a large number of inputs. In this paper, the ESVDMOR method will be used, a generalised version of SVDMOR, which was introduced by Liu & Tan (Liu, Tan, Yan, & McGaughy, 2008).

There are two steps to perform this method. First, the number of terminals is reduced by finding some correlations between the terminals thanks to Singular Value Decomposition (SVD). Secondly, the order of the SSM is reduced with a common method of Model Order Reduction. In this paper, the balanced truncation will be used. Table 14 summarizes these steps. Plain black rectangles symbolise dense matrices and hatched rectangles denote sparse matrices.

*Table 14: ESVDMOR process*

| | **ESVDMOR with balanced truncation** |
|---|---|
| Initial state space representation | $\dot{X} = \mathbf{A}\,X + \mathbf{B}\,U$<br>$Y = \mathbf{C}\,X$ |
| Step1: Decomposition of controlability and observability matrices with a SVD of output moment responses matrices. It leads to the identification of a state space model with a lower number of terminal. | $\dot{X} = \mathbf{A}\,X + \mathbf{B}\,(\underbrace{\leq U}_{U'})$<br>$Y = \mathbf{Vo}\,\underbrace{\mathbf{C}\,X}_{Y'}$ |
| Step2: Reduction of the order of the identified state space with balanced truncation method. | $\dot{X} = \mathbf{A}\,X + \mathbf{B}\,U'$<br>$Y' = \mathbf{C}\,X$ |

In the current case study, there is only one output. ESVDMOR will then just reduce the number of inputs. It will be performed on the SSM with 23 inputs.

## 7.2 Choice of the number of inputs

Liu & Tan suggest choosing the number of inputs in order to preserve significant singular value computed in step 1. However, this method was not adapted to the problem at hand. Indeed, with this criterion, only one input was preserved and the predictions of the reduced model were imprecise. So, in order to determine the number of inputs, the spectral index previously defined (Figure 9) will be used. In this figure, the balanced truncation is performed at the order 6.When the 23 inputs are preserved, the spectral index is the same as Figure 6 (case600) and Figure 7 (case900). Spectral index is quickly downgraded when the number of inputs decreases. However, it is still satisfying. To confirm that, in the following part, the results of ESVDMOR will be compared to those of simple balanced truncation.

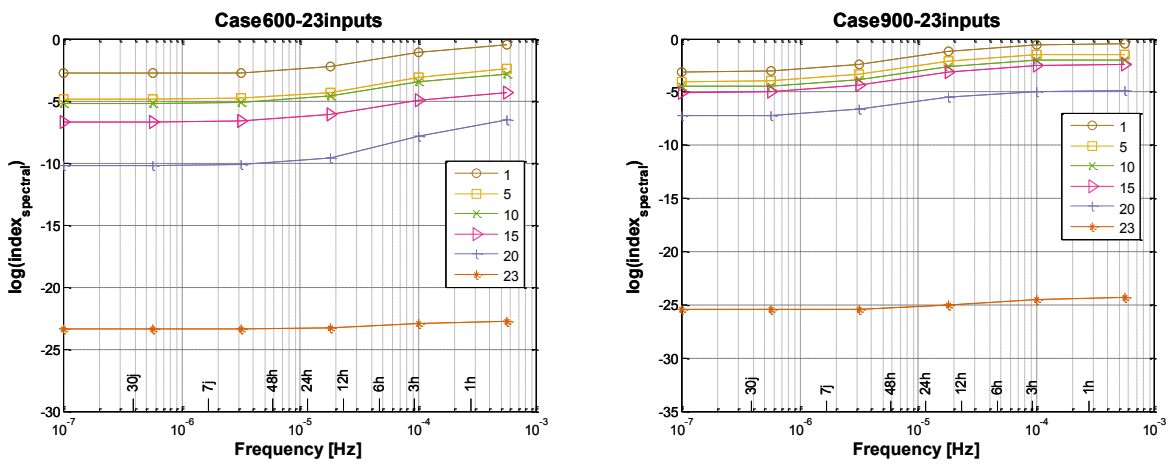


*Figure 9: Spectral indices according to the number of inputs – ESVDMOR*

## 7.3 Results

The main results of simulation with ESVDMOR are shown in Table 15. The model with 5 inputs gives results with the best compromise between computation time and results quality. However, the saving is not significant (less than 0,2s on around 50s). In fact, the step which allows computing $U'$ from U and $Y$ from $Y'$ is added in this method. So, the gain obtained thanks to the reduced number of inputs is compensated by this additional step.

*Table 15: Results of ESVDMOR - Free floating cases*

| **Method** | **Computation time** | **Case600FF $e(t)$** mean/st. dev. (°C) | **Case900FF $e(t)$** mean/st. dev. (°C) |
|---|---|---|---|
| Moore | 54,33s | -8.00e-06/7.27e-03 | -5.12e-06/6.03e-04 |
| ESVDMOR (1input) | 51,53s | 1.43e-01/8.04e-01 | 1.67e-01/7.80e-01 |
| ESVDMOR (5inputs) | 54,13s | -1.57e-01/4.97e-02 | 3.18e-01/3.30e-01 |
| ESVDMOR (10inputs) | 55,15s | -1.18e-01/3.21e-02 | 4.23e-01/3.37e-01 |
| ESVDMOR (15inputs) | 56,45s | 7.33e-02/9.49e-02 | 4.36e-01/5.78e-01 |

## 8. CONCLUSION

In this study, two methods to reduce the order of a detailed building model were used. The first was the balanced truncation. If the order is sufficient, the reduced order model will make predictions close to the detailed model. Two indicators were used to qualify the models. The spectral index gives an a priori evaluation of the adequate reduction order. The spectral analysis of the residual between the results of detailed and reduced models gives a good qualitative insight of the contribution of inputs on the residual and is as such an indication of the submodels responsible for the gaps between model results. It should, though, be used with caution when it comes to quantitative evaluations, since the order in which inputs are considered matters. The time saving of model order reduction is not significant on the test cases used, compared to the time saving obtained by the extraction of a time-invariant state-space model. The sparsity of the matrix corresponding to the linearized detailed model, and the large number of inputs of the linearized system, explain this low time saving.

Then, a second method called ESVDMOR was tested. It permits to create a state space model with a lower number of inputs and perform balanced truncation on it. However, an additional step is required. It has to be taken into account because it is computed at each time step. The results are quickly downgraded according to the number of inputs but still acceptable. Nevertheless, this method does not allow saving much time.

## ACKNOWLEDGEMENT

This research was supported by an Agence Nationale de la Recherche grant (Project MAEVIA # ANR-12-VBDU-0005).

## REFERENCES

Ademe. (2013). *Climat, air et énergie. Chiffres-clés*.

ANSI/ASHRAE Standard 140-2001, Standard method of test for the evaluation of building energy analysis computer programs. (2001).

Bruq, D., & Folliot, G. (1988). *Théorie du signal: modélisation statistique, automatique et traitement*.

Curtain, R. F., & Glover, K. (1985). Balanced realizations for infinite dimensional systems.

Dautin, S. (1997). *Réduction de modèles thermiques de bâtiments: amélioration des techniques par modélisation des sollicitations météorologiques*. Université de Poitiers.

Déqué, F., Delille, S., & Dautin, S. (1997). Réduction d'un système linéaire et invariant par la technique de Moore. Application à la thermique du bâtiment. *Revue Générale de Thermique*, *36*(3), 170–179.

Energy future, Think Efficiency. (2010). *The American Physical Society*.

Feldmann, P., & Freund, R. (1995). Efficient linear circuit analysis by Padé approximation via the Lanczos process. *IEEE Transactions on Computer-Aided Design of Integrated Circuits and Systems*, *14*(5), 639–649.

Feldmann, P., & Liu, T. (2004). Sparse and efficient reduced order modeling of linear subcircuits with large number of terminals. *IEEE/ACM International Conference on Computer Aided Design, 2004. ICCAD-2004*, 88–92.

Husaunndee, A., Lahrech, R., Vaezi-Nejad, H., & Visier, J.-C. (1997). SIMBAD: A simulation toolbox for the design and test of HVAC control systems. In *Proceedings of the 5th IBPSA Conference* (pp. 269–276).

Kim, D., & Braun, J. (2012). Reduced-order building modeling for application to model-based predictive control. *SimBuild 2012*, 554–561.

Liu, P., Tan, S., & McGaughy, B. (2007). Termmerg: an efficient terminal-reduction method for interconnect circuits. *IEEE Transactions on Computer-Aided Design of Integrated Circuits and Systems*, *26*(8), 1382–1392.

Liu, P., Tan, S. X.-D., Yan, B., & McGaughy, B. (2008). An efficient terminal and model order reduction algorithm. *Integration, the VLSI Journal*, *41*(2), 210–218.

Moore, B. (1981). Principal component analysis in linear systems: Controllability, observability, and model reduction. *IEEE Transactions on Automatic Control*, *26*(1), 17–32.

Odabasioglu, A., Celik, M., & Pileggi, L. (1997). PRIMA: passive reduced-order interconnect macromodeling algorithm. *IEEE/ACM International Conference on Computer Aided Design, 1997. ICCAD-1997*, 58–65.

Palomo, E. (2011). Résolution de problèmes thermiques de grande dimension.

Palomo, E., Bonnefous, Y., & Déqué, F. (1997). Guidance for the selection of a reduction technique for thermal models. *Proceedings of Building Simulation'97*.

Ramdani, N., Candau, Y., Dautin, S., Delille, S., Rahni, N., & Dalicieux, P. (1997). How to improve building thermal simulation programs by use of spectral analysis. *Energy and Buildings*, *25*(3), 223–242.

Sirovich, L. (1987). *Turbulence and the dynamics of coherent structures*.

Visier, J.-C. (2008). Vers des bâtiments à énergie positive. *Annales Des Mines - Réalités Industrielles*.